universe

MDPI

Communication

X-ray Redshifts for Obscured Active Galactic Nuclei with AXIS Deep and Intermediate Surveys

Alessandro Peca [1,*], Nico Cappelluti [1], Stefano Marchesi [2,3,4], Edmund Hodges-Kluck [5] and Adi Foord [6]

[1] Department of Physics, University of Miami, Coral Gables, FL 33124, USA
[2] Dipartimento di Fisica e Astronomia (DIFA), Università di Bologna, Via Gobetti 93/2, 40129 Bologna, Italy
[3] Kinard Laboratory of Physics, Department of Physics and Astronomy, Clemson University, Clemson, SC 29634, USA
[4] INAF—Osservatorio di Astrofisica e Scienza dello Spazio di Bologna, Via Piero Gobetti 93/3, 40129 Bologna, Italy
[5] NASA Goddard Space Flight Center Code 662, Greenbelt, MD 20771, USA
[6] Department of Physics, University of Maryland Baltimore County, 1000 Hilltop Cir, Baltimore, MD 21250, USA
* Correspondence: peca.alessandro@gmail.com

Abstract: This study presents the capabilities of the AXIS telescope in estimating redshifts from X-ray spectra alone (X-ray redshifts, XZs). Through extensive simulations, we establish that AXIS observations enable reliable XZ estimates for more than 5500 obscured active galactic nuclei (AGNs) up to redshift $z\sim6$ in the proposed deep (7 Ms) and intermediate (375 ks) surveys. Notably, at least 1600 of them are expected to be in the Compton-thick regime ($\log N_H/\mathrm{cm}^{-2} \geq 24$), underscoring the pivotal role of AXIS in sampling these elusive objects that continue to be poorly understood. XZs provide an efficient alternative for optical/infrared faint sources, overcoming the need for time-consuming spectroscopy, the potential limitations of photometric redshifts, and potential issues related to multi-band counterpart association. This approach will significantly enhance the accuracy of constraints on the X-ray luminosity function and obscured AGN fractions up to high redshifts. This white paper is part of a series commissioned for the AXIS Probe Concept Mission; additional AXIS white papers can be found at the AXIS website.

Keywords: active galactic nuclei; X-rays; surveys; probes; redshifts

check for updates

Citation: Peca, A.; Cappelluti, N.; Marchesi, S.; Hodges-Kluck, E.; Foord, A. X-ray Redshifts for Obscured Active Galactic Nuclei with AXIS Deep and Intermediate Surveys. *Universe* **2024**, *10*, 245. https://doi.org/10.3390/universe10060245

Academic Editor: Stefano Carniani

Received: 18 April 2024
Revised: 14 May 2024
Accepted: 22 May 2024
Published: 1 June 2024

Copyright: © 2024 by the authors. Licensee MDPI, Basel, Switzerland. This article is an open access article distributed under the terms and conditions of the Creative Commons Attribution (CC BY) license (https://creativecommons.org/licenses/by/4.0/).

1. Introduction

Redshifts play a crucial role in the study of the properties and evolution of active galactic nuclei (AGNs). To determine the redshift of an AGN, most solid measurements can be obtained through the spectroscopic identification of optical/near-infrared (ONIR) emission lines. However, spectroscopic redshift (spec-z) quality relies on good signal-to-noise spectra, which can be resource-intensive in terms of exposure times, especially for faint and distant AGNs. An alternative to spec-zs is to compute photometric redshifts (photo-zs) through spectral energy distribution (SED) fitting. This is a more easily accessible method which relies on multi-wavelength observations by comparing object fluxes in different filters with synthetic models. However, accurate photometric redshifts may be challenging to obtain for AGNs because of the complex nature of their SEDs and the limited availability of filters needed to obtain reliable estimates. This challenge is further compounded by the potential dilution of the AGNs' emissions by concurrent galaxy radiation (e.g., [1,2]).

In recent years, a relatively new technique based on X-ray spectra has been extensively explored to determine the redshifts of AGNs. These redshift estimates (X-ray redshifts, XZs) were successfully tested for an obscured AGN [3–5] which may be extremely faint at ONIR wavelengths due to gas and dust along the line of sight. On the contrary, X-ray

photons can more easily escape heavy column densities ($\log N_H/\mathrm{cm}^{-2} > 23$, e.g., [6,7]), providing a valuable alternative to AGNs that are challenging to observe spectroscopically and photometrically. Therefore, XZs offer a complementary approach that does not require ONIR datasets and avoids the complexities associated with multi-band counterpart associations (e.g., [8–10]). However, as with other redshift methods, even XZs rely on the quality of data. Current X-ray observatories such as *Chandra* and *XMM*-Newton provide excellent spectra on-axis (i.e., in the center of their field of view), but as we move off-axis, the PSF broadens and distorts very quickly, drastically reducing the quality of the spectra and therefore negatively affecting the performance of the XZ method. In contrast, with a stable angular resolution across its entire field of view, the AXIS telescope can capture a large amount of high-quality spectra within a single pointing, more than ever before. This, coupled with its large effective area [11–13], makes it the ideal instrument for measuring XZs. In this white paper, we explore the capabilities of AXIS in deriving the XZs of obscured AGNs in the planned deep (7 Ms) and intermediate (375 ks) surveys [14–16], by focusing on the low-photon statistics regime to investigate the limits of this technique. For details on the expected surveys and observations, we refer to the main AXIS papers [13–15].

2. Materials and Methods

The methods presented in this section were carried out using a procedure similar to that in [4]. In brief, we simulated the expected AXIS spectra of obscured AGNs ($\log N_H \geq 22$) in order to derive their redshifts through an analysis of X-ray spectra. All the simulations were conducted using PyXSPEC v2.1.1 (equivalent to XSPEC v12.13.0 [17]). We adopted a double-power-law model (ZPHABS × ZPOWERLW + ZPOWERLW in XSPEC) with a fixed intrinsic photon index $\Gamma = 1.9$ and a secondary power-law normalization free to vary up to 20% of the primary power-law normalization (as observed in X-ray surveys (e.g., [18,19])). The absorbing column density, N_H, was modeled to represent the total absorption due to cold (or neutral) gas along the line of sight, known as the predominant mechanism of absorption in AGNs and their host galaxies (e.g., [20–22], see also Appendix B). The Fe Kα emission line was also modeled with a redshifted Gaussian line (ZGAUSS) at 6.4 keV in the rest frame, with a width of $\sigma = 10$ eV. Different line normalizations were used to obtain a canonical range of rest-frame equivalent widths between 10 eV and 2 keV as a function of N_H (e.g., [23,24]). An additional absorption component (PHABS) with a fixed value of $N_H = 1.8 \times 10^{20}$ cm^{-2}, corresponding to the average Galactic absorption at a high latitude, was added. The free parameters were the two power-law normalizations, N_H, line normalization, and redshift. We discuss the effects of assuming different models in Appendix B.

To reproduce what is observed in intermediate-to-deep X-ray surveys (e.g., [25,26]), we simulated column densities from $\log N_H = 22$ to 25 with a step of 0.5, redshifts up to 9 with a step of 0.5, and different power-law normalizations to obtain a number of net counts (0.5–10 keV band) of up to 150. For each parameter combination, we simulated 200 spectra. The simulations were also repeated by excluding the Fe Kα emission line to mimic cases in which no line is detected. The expected background, which comprises both particle (non-X-ray) and astrophysical components, was properly modeled (see Appendix A for details) and associated with the simulated spectra. The most recent AXIS responses, ARF and RMF, were applied. The simulated spectra were binned to a minimum of 1 cts/bin to avoid empty channels, and Cash statistics [27] were applied. Following [4], after a first fit to assess the free parameters, the best-fit redshift estimates (XZs) were evaluated using the STEPPAR command. This allowed for an evaluation of the possible best-fit solutions by running consecutive fits as a function of one or more parameters. We ran it as a function of z in the range [0–11], with a step of 0.01. The best-fit XZs were then determined to be the minimum value in the resulting statistical distributions. Finally, the model's best-fit parameters were then compared to the simulated values as described in Section 3. An example of this procedure is shown in Figure 1.

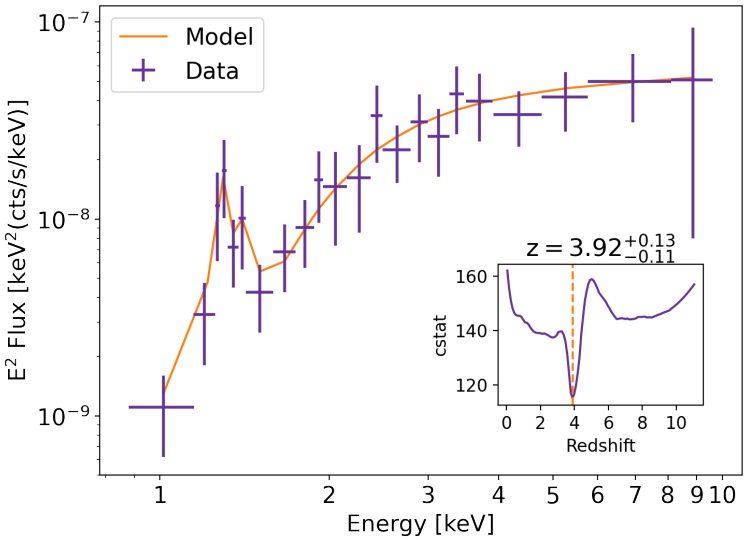


Figure 1. The predicted unfolded AXIS spectrum for a Compton-thick AGN at $z = 4$, with $\log N_H/\mathrm{cm}^{-2} = 24$ and $\log L_X/\mathrm{erg\,s}^{-1} = 43.5$. The spectrum (purple points) was simulated assuming a double-power-law model with the secondary power-law normalization as 3% of the primary one (orange curve). The number of net counts is 146. The inset in the figure shows the result obtained by the STEPPAR command on the redshift parameter. The minimum (orange dashed line) marks the best-fit XZ value, $z = 3.92^{+0.13}_{-0.11}$, which agrees well with the simulated redshift.

3. Results

In this section, we show the main results of our simulations. We applied the method described in [4] to determine the feasibility of XZs with AXIS. This method provides the XZ success rate maps as functions of redshifts, the number of counts, and absorption column density (N_H). The success rate, or match percentage (MP), is defined as follows:

$$\mathrm{MP}(cts, z, N_\mathrm{H}) = \frac{N(z \pm \Delta z)}{N_\mathrm{sim}} \quad (1)$$

This quantity represents the percentage of simulated sources for which the spectral fitting successfully recovered a redshift that agrees, within the errors, with the simulated value (as well as for N_H and power-law normalizations). In other words, the MP shows how well XZs can be estimated as functions of redshifts, counts, and N_H by using X-ray spectra alone. It is worth mentioning that the MP is also a function of the photon index Γ, but for commonly accepted values ($\Gamma = 1.9 \pm 0.2$, e.g., [28,29]), the effect on the MP is negligible [4]. As a conservative approach [3,5], we rejected estimates where the derived XZ was consistent with the simulated one, within the errors, but where $|\Delta z| > 0.15(1 + z_{sim})$. This also applies when XZ estimates were upper or lower limits.

In Figure 2, we present the results obtained for a double-power-law model with $\Gamma = 1.9$, $\log N_H/\mathrm{cm}^{-2}$ in the range 22–25, and where we included the 6.4 keV Fe Kα emission line (see details in Section 2). From the three maps, it is clear how increasing the levels of absorption can provide more accurate XZ results. The reason is that the XZ estimates are driven by the 6.4 keV Fe Kα emission line and the absorption features (the 7.1 keV Fe Kα absorption edge and photoelectric absorption), which become more prominent with increasing absorption and therefore more easily identifiable via spectral fitting (e.g., [3,30]). In addition to highlighting the prominence of the main features in the X-ray spectrum when obscuration increases, these simulations provide valuable insight into the probability of accurately determining the redshift of these AGNs by analyzing their X-ray spectra alone. We chose an MP threshold $\geq$ of 50% as the likelihood of obtaining a reliable XZ estimate. Refs. [4,19] showed that this threshold is a fair compromise between having a large enough sample and spectral fit accuracy. In particular, our results show that

it is possible to compute reliable XZs up to $z{\sim}9$ for $\log N_H/\mathrm{cm}^{-2} = 25$ and a number of counts down to ∼20. These numbers are expected to change when other AGN models are used [4,19]. However, as assumed in other X-ray surveys (e.g., [24,26]), our chosen model is a good representation of the overall shape of an obscured AGN. For completeness, we discuss the effects of assuming other models in Appendix B.

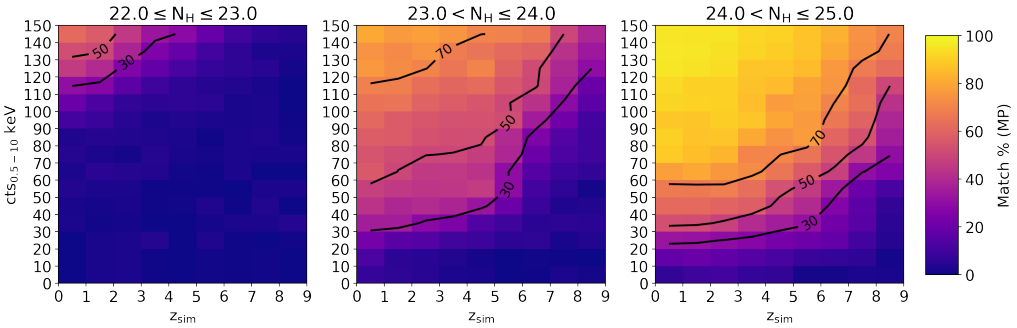


Figure 2. Match percentage (MP) maps as a function of redshift and number of counts in the 0.5–10 keV band for three $\log N_H$ bins. In this simulation, we used a double-power-law model with the 6.4 keV Fe Kα emission line and an exposure time of 7 Ms (see details in Section 2). The solid black contours represent MP = 30, 50, and 70%, respectively.

4. Discussion

AXIS is expected to provide valuable X-ray redshift measurements, allowing for in-depth studies of X-ray-obscured AGN populations, especially for those in the Compton-thick ($\log N_H/\mathrm{cm}^{-2} \geq 24$) regime. By using the most up-to-date simulations for the deep (7 Ms) and intermediate (375 ks) AXIS surveys [13,14], we can predict how many reliable XZs we will be able to estimate. Figure 3 shows our predictions for both cases in which the 6.4 keV Kα emission line is included in the model or not. We can estimate reliable XZs for a number of obscured ($\log N_H/\mathrm{cm}^{-2} > 22$) AGNs between ∼5500 and 6500 and for Compton-thick AGNs between 1600 and 2000. Of these, around six Compton-thick AGNs are in the redshift bin 4 to 6.5. Furthermore, as shown by Figure 2, with additional observations, it will be possible to determine XZs even at higher redshifts as long as enough photons are detected. It is worth noting that our simulated mock datasets do not assume a redshift-dependent evolution of the $\log N_H/\mathrm{cm}^{-2} > 23$ population. However, numerous observations suggest that as we look at high redshifts, this population could make up as much as 90% (e.g., [18,31]), possibly due to the interstellar medium contribution to the overall absorption (e.g., [21,22,32]). As a result, the numbers we present, especially for $z > 2$, should be considered conservative lower limits.

Our results offer an alternative solution for the redshift determination of X-ray sources. Notably, this approach circumvents the reliance on ONIR multi-band counterparts, which is becoming increasingly challenging with the advent of new data from instruments like the James Webb Space Telescope (JWST), which offers a superior angular resolution compared to X-rays. As a result, our method will substantially refine constraints on the X-ray luminosity function (XLF) and obscured AGN fractions up to redshift 6. In particular, we will be able to determine a solid Compton-thick fraction up to redshift 4 and place constraints up to z∼6. This holds particular importance because current work shows discrepancies in the Compton-thick fraction even in the local universe (e.g., [18,31,33,34]) and, ata high redshift ($z > 4$), the use of extrapolations or XLFs characterized by notable uncertainties is common due to a lack of strong empirical support.

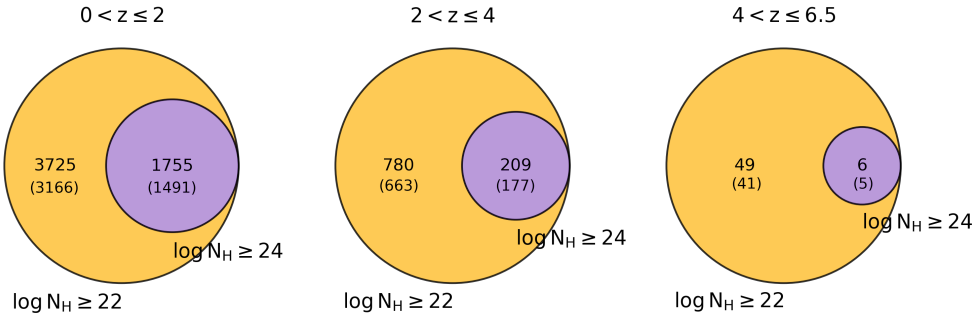


Figure 3. Predicted number of reliable XZs in the combined deep (7 Ms) and intermediate (375 ks) planned AXIS surveys [13,15,16]. The three Venn diagrams show different redshift bins, while the orange and purple circles show the expected numbers of XZs for $\log N_H/\mathrm{cm}^{-2} \geq 22$ and 24, respectively. The provided numbers represent our projections based on a model with a 6.4 keV Kα emission line, while the values within the parentheses indicate the scenario in which no emission line is detected.

5. Conclusions

We showed in this work how AXIS is poised to make significant contributions to the study of AGN populations, especially obscured AGNs, through accurate X-ray redshift estimations. Our simulations suggest that AXIS can accurately estimate XZs for obscured AGNs up to redshift $z\sim6$ in the planned deep and intermediate surveys. Specifically, AXIS will be able to obtain X-ray spectra with enough photons to make XZ estimates for more than 5500 obscured AGNs, of which at least $\sim$1600 are in the Compton-thick regime. Moreover, with additional observations, it would be possible to determine XZs even at higher redshifts as long as enough photons will be detected. This capability will substantially contribute to our understanding of the characteristics and evolution of heavily obscured and elusive AGNs, which bear critical importance in population studies. With the presented predictions, our approach will significantly improve the accuracy of XLFs and obscured AGN fractions up to redshift $\sim$6 and beyond. This advancement will address critical gaps in our understanding of obscured AGNs, both locally and at high redshifts ($z \gtrsim 4$), where current discrepancies may be explained by the lack of solid observational evidence that AXIS will instead provide.

Author Contributions: Conceptualization, A.P. and N.C.; methodology, A.P.; software, S.M. and E.H.-K.; validation, A.P., N.C. and A.F.; formal analysis, A.P.; investigation, A.P.; resources, S.M. and E.H.-K.; data curation, A.P. and S.M.; writing—original draft preparation, A.P.; writing—review and editing, N.C. and A.F.; visualization, A.P.; supervision, N.C. and A.F.; project administration, N.C. and A.F.; funding acquisition, N.C. All authors have read and agreed to the published version of the manuscript.

Funding: This research received no external funding.

Data Availability Statement: Data are contained within the article.

Acknowledgments: We kindly acknowledge the AXIS team for their outstanding scientific and technical work over the past year. This work is the result of several months of discussion in the AXIS-AGN SWG.

Conflicts of Interest: The authors declare no conflicts of interest.

Abbreviations

The following abbreviations are used in this manuscript:

AGN	active galactic nuclei
CXB	Cosmic X-ray background
MP	Match percentage
NXB	Particle background
ONIR	Optical and near-IR
PSF	Point spread function
SED	Spectral energy distribution
XLF	X-ray luminosity function
XZ	X-ray redshift

Appendix A. Background Simulation

The expected background combines two main components: astrophysical and particle (NXB) backgrounds. For the latter, we used an empirical model based on the observed Suzaku XIS1 NXB spectrum [35] and scaled it to what is expected for AXIS in a low-Earth orbit. It was modeled with a series of instrumental Gaussian emission lines and three power-law components to mimic the continuum shape. Since the NXB does not depend on the effective area of the instrument, it was not convolved with the ARF during the simulations. The astrophysical background is the contribution of the unresolved X-ray background (CXB) and the galactic foreground emission (the local hot bubble and Milky Way hot halo). To model its contribution, we used the models provided by [36,37], respectively.

Appendix B. Model Complexity

An important factor to consider when dealing with low-photon statistics is the complexity of the model used to determine XZs. In general, with low-quality spectra, only simple models are used (e.g., [7,26,30,38]) as it becomes too challenging to fit the larger number of components present in complex models. In addition, fixing many parameters to the default values makes the shape of complex models similar to simple ones, leading to consistent results but requiring more computational time. In Section 2, we show the results obtained with a double-power-law model. Ref. [4] show how using a more simple, single-power-law model and a more complex model such as MYTorus [39], change the MP results by no more than $\pm$15%. It is also worth mentioning that the spectral shape may be influenced by additional cold and warm components along the line of sight (e.g., warm–hot intergalactic medium, WHIM; circumgalactic medium, CGM). However, results from both simulations and observations showed that these contributions can be considered negligible compared to the rest-frame absorption [40,41]; in addition, they are also extremely difficult to detect with spectral resolutions similar to the AXIS telescope [42,43]. Given these reasons, we can conclude that assuming simple models for the redshift estimate of obscured AGN is a reasonable choice. The main spectral features, such as the Fe Kα emission line at 6.4 keV and the main absorption features, are those that drive the XZ estimates and are already included in these models. Therefore, it is not necessary to add more complexity to the models to derive XZs.

Iron Kα Emission Line and Absorption Features

XZ estimates are driven by a combination of emission (notably the Fe 6.4 keV Kα emission line) and absorption features (primarily the 7.1 Fe Kα absorption edge and the photoelectric cut-off). However, in situations of limited photon statistics, the detection of the Fe 6.4 keV Kα emission line is not always successful (e.g., [7,26]). To account for such scenarios, we ran the simulations again without the Gaussian component. On average, this modification led to a decrease of approximately $\sim$10–15% in the MP. This outcome can be explained by the fact that the larger uncertainties derived from absorption features can only cause some XZs to not meet the criterion of $|\Delta z| > 0.15(1 + z_{sim})$. In fact, although ab-

sorption is the primary determinant for an XZ, the narrower profile of the Fe 6.4 keV Kα feature allows for smaller errors [3,4,7]. During the computation of uncertainties, XSPEC evaluates the statistics around the best-fit solution and, consequently, when an emission line is identified, the X-ray redshift likelihood experiences a rapid decline before and after the best-fit value, resulting in smaller uncertainties. In contrast, when only broad absorption features are identified, the uncertainties on XZs are larger.

References

1. Salvato, M.; Hasinger, G.; Ilbert, O.; Zamorani, G.; Brusa, M.; Scoville, N.Z.; Rau, A.; Capak, P.; Arnouts, S.; Aussel, H.; et al. Photometric Redshift and Classification for the XMM-COSMOS Sources. *Astrophys. J.* **2009**, *690*, 1250–1263. [CrossRef]
2. Salvato, M.; Ilbert, O.; Hoyle, B. The many flavours of photometric redshifts. *Nat. Astron.* **2019**, *3*, 212–222. [CrossRef]
3. Simmonds, C.; Buchner, J.; Salvato, M.; Hsu, L.T.; Bauer, F.E. XZ: Deriving redshifts from X-ray spectra of obscured AGN. *Astron. Astrophys.* **2018**, *618*, A66. [CrossRef]
4. Peca, A.; Vignali, C.; Gilli, R.; Mignoli, M.; Nanni, R.; Marchesi, S.; Bolzonella, M.; Brusa, M.; Cappelluti, N.; Comastri, A.; et al. X-ray Redshifts for Obscured AGN: A Case Study in the J1030 Deep Field. *Astrophys. J.* **2021**, *906*, 90. [CrossRef]
5. Sicilian, D.; Civano, F.; Cappelluti, N.; Buchner, J.; Peca, A. X-ray Redshifts of Obscured Chandra Source Catalog Active Galactic Nuclei. *Astrophys. J.* **2022**, *936*, 39. [CrossRef]
6. Buchner, J.; Georgakakis, A.; Nandra, K.; Brightman, M.; Menzel, M.L.; Liu, Z.; Hsu, L.T.; Salvato, M.; Rangel, C.; Aird, J.; et al. Obscuration-dependent Evolution of Active Galactic Nuclei. *Astrophys. J.* **2015**, *802*, 89. [CrossRef]
7. Signorini, M.; Marchesi, S.; Gilli, R.; Brusa, M.; Comastri, A.; D'Amato, Q.; Iwasawa, K.; Lanzuisi, G.; Mazzolari, G.; Mignoli, M.; et al. X-ray properties and obscured fraction of AGN in the J1030 Chandra field. *arXiv* **2023**, arXiv:2305.13368.
8. Brusa, M.; Zamorani, G.; Comastri, A.; Hasinger, G.; Cappelluti, N.; Civano, F.; Finoguenov, A.; Mainieri, V.; Salvato, M.; Vignali, C.; et al. The XMM-Newton Wide-Field Survey in the COSMOS Field. III. Optical Identification and Multiwavelength Properties of a Large Sample of X-ray-Selected Sources. *Astrophys. J.* **2007**, *172*, 353–367. [CrossRef]
9. Nanni, R.; Gilli, R.; Vignali, C.; Mignoli, M.; Peca, A.; Marchesi, S.; Annunziatella, M.; Brusa, M.; Calura, F.; Cappelluti, N.; et al. The deep Chandra survey in the SDSS J1030+0524 field. *Astron. Astrophys.* **2020**, *637*, A52. [CrossRef]
10. Salvato, M.; Buchner, J.; Budavári, T.; Dwelly, T.; Merloni, A.; Brusa, M.; Rau, A.; Fotopoulou, S.; Nandra, K. Finding counterparts for all-sky X-ray surveys with NWAY: A Bayesian algorithm for cross-matching multiple catalogues. *Mon. Not. R. Astron. Soc.* **2018**, *473*, 4937–4955. [CrossRef]
11. Mushotzky, R.; Aird, J.; Barger, A.J.; Cappelluti, N.; Chartas, G.; Corrales, L.; Eufrasio, R.; Fabian, A.C.; Falcone, A.D.; Gallo, E.; et al. The Advanced X-ray Imaging Satellite. *arXiv* **2019**, arXiv:1903.04083.
12. Mushotzky, R. AXIS: A probe class next generation high angular resolution X-ray imaging satellite. In *Proceedings of the Space Telescopes and Instrumentation 2018: Ultraviolet to Gamma Ray*; den Herder, J.W.A., Nikzad, S., Nakazawa, K., Eds.; Society of Photo-Optical Instrumentation Engineers (SPIE) Conference Series; SPIE: Bellingham, WA USA, 2018; Volume 10699, p. 1069929. [CrossRef]
13. Reynolds, C.S.; Kara, E.A.; Mushotzky, R.F.; Ptak, A.; Koss, M.J.; Williams, B.J.; Allen, S.W.; Bauer, F.E.; Bautz, M.; Bogadhee, A.; et al. Overview of the advanced x-ray imaging satellite (AXIS). In *Proceedings of the UV, X-Ray, and Gamma-Ray Space Instrumentation for Astronomy XXIII*; Siegmund, O.H., Hoadley, K., Eds.; Society of Photo-Optical Instrumentation Engineers (SPIE) Conference Series; SPIE: Bellingham, WA, USA, 2023; Volume 12678, p. 126781E. [CrossRef]
14. Marchesi, S.; Gilli, R.; Lanzuisi, G.; Dauser, T.; Ettori, S.; Vito, F.; Cappelluti, N.; Comastri, A.; Mushotzky, R.; Ptak, A.; et al. Mock catalogs for the extragalactic X-ray sky: Simulating AGN surveys with ATHENA and with the AXIS probe. *Astron. Astrophys.* **2020**, *642*, A184. [CrossRef]
15. Cappelluti, N.; Foord, A.; Marchesi, S.; Pacucci, F.; Ricarte, A.; Habouzit, M.; Vito, F.; Powell, M.; Koss, M.; Mushotzky, R.; et al. Surveying the onset and evolution of supermassive black holes at high-z with AXIS. *arXiv* **2023**, arXiv:2311.07669.
16. Foord, A.; Cappelluti, N.; Liu, T.; Volonteri, M.; Habouzit, M.; Pacucci, F.; Marchesi, S.; Chen, N.; Di Matteo, T.; Mallick, L.; et al. Tracking SMBH mergers from kpc to sub-pc scales with AXIS. *arXiv* **2023**, arXiv:2311.07664.
17. Arnaud, K.A. XSPEC: The First Ten Years. In *Proceedings of the Astronomical Data Analysis Software and Systems V*; Jacoby, G.H., Barnes, J., Eds.; Astronomical Society of the Pacific Conference Series; 1996; Volume 101, p. 17.
18. Ricci, C.; Trakhtenbrot, B.; Koss, M.J.; Ueda, Y.; Del Vecchio, I.; Treister, E.; Schawinski, K.; Paltani, S.; Oh, K.; Lamperti, I.; et al. BAT AGN Spectroscopic Survey. V. X-ray Properties of the Swift/BAT 70-month AGN Catalog. *Astrophys. J.* **2017**, *233*, 17. [CrossRef]
19. Peca, A.; Cappelluti, N.; Urry, C.M.; LaMassa, S.; Marchesi, S.; Ananna, T.T.; Baloković, M.; Sanders, D.; Auge, C.; Treister, E.; et al. On the Cosmic Evolution of AGN Obscuration and the X-Ray Luminosity Function: XMM-Newton and Chandra Spectral Analysis of the 31.3 deg^2 Stripe 82X. *Astrophys. J.* **2023**, *943*, 162. [CrossRef]
20. Hickox, R.C.; Alexander, D.M. Obscured Active Galactic Nuclei. *Annu. Rev. Astron. Astrophys.* **2018**, *56*, 625–671. [CrossRef]
21. D'Amato, Q.; Gilli, R.; Vignali, C.; Massardi, M.; Pozzi, F.; Zamorani, G.; Circosta, C.; Vito, F.; Fritz, J.; Cresci, G.; et al. Dust and gas content of high-redshift galaxies hosting obscured AGN in the Chandra Deep Field-South. *Astron. Astrophys.* **2020**, *636*, A37. [CrossRef]

22. Gilli, R.; Norman, C.; Calura, F.; Vito, F.; Decarli, R.; Marchesi, S.; Iwasawa, K.; Comastri, A.; Lanzuisi, G.; Pozzi, F.; et al. Supermassive black holes at high redshift are expected to be obscured by their massive host galaxies' interstellar medium. *Astron. Astrophys.* **2022**, *666*, A17. [CrossRef]
23. Ghisellini, G.; Haardt, F.; Matt, G. The contribution of the obscuring torus to the X-ray spectrum of Seyfert galaxies: A test for the unification model. *Mon. Not. R. Astron. Soc.* **1994**, *267*, 743–754. [CrossRef]
24. Lanzuisi, G.; Ranalli, P.; Georgantopoulos, I.; Georgakakis, A.; Delvecchio, I.; Akylas, T.; Berta, S.; Bongiorno, A.; Brusa, M.; Cappelluti, N.; et al. Compton thick AGN in the XMM-COSMOS survey. *Astron. Astrophys.* **2015**, *573*, A137. [CrossRef]
25. Liu, T.; Tozzi, P.; Wang, J.X.; Brandt, W.N.; Vignali, C.; Xue, Y.; Schneider, D.P.; Comastri, A.; Yang, G.; Bauer, F.E.; et al. X-ray Spectral Analyses of AGNs from the 7Ms Chandra Deep Field-South Survey: The Distribution, Variability, and Evolutions of AGN Obscuration. *Astrophys. J.* **2017**, *232*, 8. [CrossRef]
26. Marchesi, S.; Lanzuisi, G.; Civano, F.; Iwasawa, K.; Suh, H.; Comastri, A.; Zamorani, G.; Allevato, V.; Griffiths, R.; Miyaji, T.; et al. The Chandra COSMOS-Legacy Survey: Source X-ray Spectral Properties. *Astrophys. J.* **2016**, *830*, 100. [CrossRef]
27. Cash, W. Parameter estimation in astronomy through application of the likelihood ratio. *Astrophys. J.* **1979**, *228*, 939–947. [CrossRef]
28. Nandra, K.; Pounds, K.A. GINGA observations of the X-ray spectra of Seyfert galaxies. *Mon. Not. R. Astron. Soc.* **1994**, *268*, 405–429. [CrossRef]
29. Piconcelli, E.; Jimenez-Bailón, E.; Guainazzi, M.; Schartel, N.; Rodríguez-Pascual, P.M.; Santos-Lleó, M. The XMM-Newton view of PG quasars. I. X-ray continuum and absorption. *Astron. Astrophys.* **2005**, *432*, 15–30. [CrossRef]
30. Iwasawa, K.; Gilli, R.; Vignali, C.; Comastri, A.; Brandt, W.N.; Ranalli, P.; Vito, F.; Cappelluti, N.; Carrera, F.J.; Falocco, S.; et al. The XMM deep survey in the CDF-S. II. A 9–20 keV selection of heavily obscured active galaxies at z > 1.7. *Astron. Astrophys.* **2012**, *546*, A84. [CrossRef]
31. Ananna, T.T.; Treister, E.; Urry, C.M.; Ricci, C.; Kirkpatrick, A.; LaMassa, S.; Buchner, J.; Civano, F.; Tremmel, M.; Marchesi, S. The Accretion History of AGNs. I. Supermassive Black Hole Population Synthesis Model. *Astrophys. J.* **2019**, *871*, 240. [CrossRef]
32. Circosta, C.; Vignali, C.; Gilli, R.; Feltre, A.; Vito, F.; Calura, F.; Mainieri, V.; Massardi, M.; Norman, C. X-ray emission of z > 2.5 active galactic nuclei can be obscured by their host galaxies. *Astron. Astrophys.* **2019**, *623*, A17. [CrossRef]
33. Torres-Albà, N.; Marchesi, S.; Zhao, X.; Ajello, M.; Silver, R.; Ananna, T.T.; Baloković, M.; Boorman, P.B.; Comastri, A.; Gilli, R.; et al. Compton-thick AGN in the NuSTAR Era VI: The Observed Compton-thick Fraction in the Local Universe. *Astrophys. J.* **2021**, *922*, 252. [CrossRef]
34. Sengupta, D.; Marchesi, S.; Vignali, C.; Torres-Albà, N.; Bertola, E.; Pizzetti, A.; Lanzuisi, G.; Salvestrini, F.; Zhao, X.; Gaspari, M.; et al. Compton-thick AGN in the NuSTAR Era X: Analysing seven local CT-AGN candidates. *Astron. Astrophys.* **2023**, *676*, A103. [CrossRef]
35. Tawa, N.; Hayashida, K.; Nagai, M.; Nakamoto, H.; Tsunemi, H.; Yamaguchi, H.; Ishisaki, Y.; Miller, E.D.; Mizuno, T.; Dotani, T.; et al. Reproducibility of Non-X-ray Background for the X-ray Imaging Spectrometer aboard Suzaku. *Publ. Astron. Soc. Jpn.* **2008**, *60*, S11. [CrossRef]
36. Cappelluti, N.; Hasinger, G.; Brusa, M.; Comastri, A.; Zamorani, G.; Böhringer, H.; Brunner, H.; Civano, F.; Finoguenov, A.; Fiore, F.; et al. The XMM-Newton Wide-Field Survey in the COSMOS Field. II. X-ray Data and the logN-logS Relations. *Astrophys. J.* **2007**, *172*, 341–352. [CrossRef]
37. Bluem, J.; Kaaret, P.; Kuntz, K.D.; Jahoda, K.M.; Koutroumpa, D.; Hodges-Kluck, E.J.; Fuller, C.A.; LaRocca, D.M.; Zajczyk, A. Widespread Detection of Two Components in the Hot Circumgalactic Medium of the Milky Way. *Astrophys. J.* **2022**, *936*, 72. [CrossRef]
38. Vito, F.; Brandt, W.N.; Yang, G.; Gilli, R.; Luo, B.; Vignali, C.; Xue, Y.Q.; Comastri, A.; Koekemoer, A.M.; Lehmer, B.D.; et al. High-redshift AGN in the Chandra Deep Fields: The obscured fraction and space density of the sub-L_* population. *Mon. Not. R. Astron. Soc.* **2018**, *473*, 2378–2406. [CrossRef]
39. Murphy, K.D.; Yaqoob, T. An X-ray spectral model for Compton-thick toroidal reprocessors. *Mon. Not. R. Astron. Soc.* **2009**, *397*, 1549–1562. [CrossRef]
40. Campana, S.; Salvaterra, R.; Ferrara, A.; Pallottini, A. Missing cosmic metals revealed by X-ray absorption towards distant sources. *Astron. Astrophys.* **2015**, *575*, A43. [CrossRef]
41. Arcodia, R.; Campana, S.; Salvaterra, R.; Ghisellini, G. X-ray absorption towards high-redshift sources: Probing the intergalactic medium with blazars. *Astron. Astrophys.* **2018**, *616*, A170. [CrossRef]
42. Nicastro, F.; Krongold, Y.; Mathur, S.; Elvis, M. A decade of warm hot intergalactic medium searches: Where do we stand and where do we go? *Astron. Nachr.* **2017**, *338*, 281–286. [CrossRef]
43. Nicastro, F.; Kaastra, J.; Krongold, Y.; Borgani, S.; Branchini, E.; Cen, R.; Dadina, M.; Danforth, C.W.; Elvis, M.; Fiore, F.; et al. Observations of the missing baryons in the warm-hot intergalactic medium. *Nature* **2018**, *558*, 406–409. [CrossRef] [PubMed]

Disclaimer/Publisher's Note: The statements, opinions and data contained in all publications are solely those of the individual author(s) and contributor(s) and not of MDPI and/or the editor(s). MDPI and/or the editor(s) disclaim responsibility for any injury to people or property resulting from any ideas, methods, instructions or products referred to in the content.